PART II

ACTUATORS

Magnetic Actuators and Sensors, Second Edition. John R. Brauer.

CHAPTER 7

Magnetic Actuators Operated by DC

Magnetic actuators use magnetic fields to transform electrical energy into mechanical energy. Thus they are a type of *transducer*, which is any device that transforms one type of energy into another [1]. However, the mechanical motion of the magnetic actuators in this book is over a limited range of motion. This limited range is commonly assumed for actuators, unlike electric motors and other rotary electromagnetic machines, which have large unlimited motion over multiple revolutions. This part of the book, Part II, is devoted to magnetic actuators.

This chapter discusses in detail the most common types of magnetic actuators operated by direct current, in the following order: solenoid actuators, voice coil actuators, other linear actuators, proportional actuators, rotary actuators, magnetic bearings and couplings, and magnetic separators.

7.1 SOLENOID ACTUATORS

Solenoid actuators have a *solenoidal coil*, which is a coil of wire wound to a shape that is sometimes cylindrical. All solenoid actuators also have a steel *armature*, a term for the moving part. In solenoid actuators, the armature moves along a straight line and thus produces *linear motion*. A common use of solenoid actuators is to move a mechanical switch for large voltages and currents. Since the current supplied to the solenoid coil is much smaller than the current being switched, the solenoid and switch form a *relay* or *contactor*.

7.1.1 Clapper Armature

A solenoid actuator with a *clapper* armature functions similar to a clapping hand. The armature acts like one hand that is drawn by a magnetic force to the second hand. Because the second "hand" is stationary, it is called the *stator*.

Like a clapping hand, the clapper armature usually contacts the stator at two areas. In one area, magnetic flux enters the armature, while it leaves the armature through the other area, producing useful magnetic force over both areas. Since magnetic flux

Magnetic Actuators and Sensors, Second Edition. John R. Brauer.

must always both enter and leave the armature (or any other volume as discussed in Chapter 1), the clapper armature is often more compact than other designs. The clapper may be either flat, like a flat hand, or may have ridges, like a cupped hand.

The coil may be excited by either a DC voltage (and current) or by an AC voltage (and current). This chapter deals only with actuators operated by DC, while AC actuators are discussed in the next chapter. However, any such voltage (and current) must be turned on and off at some time in the past and future, and such transient effects are discussed in Chapter 9.

An example of a DC clapper solenoid is shown in Figure 7.1a. It is somewhat similar to the Eaton Cutler-Hammer AC solenoid [2] shown in Chapter 4. Its magnetic flux pattern computed by finite-element analysis is shown in Figure 7.1b.

As shown in the solenoid of Figure 7.1, the clapper and the stator can be made of steel laminations. Laminating the steel minimizes eddy current effects that reduce force and increase power loss. If laminations are used, they are usually stacked to form a geometry that must be two dimensional (2D), or planar.

Instead of planar geometry, axisymmetric geometry is very common. Solenoidal coils are often cylindrical and thus axisymmetric. If these coils are surrounded by axisymmetric steel, an axisymmetric solenoid is created. However, since axisymmetric geometries cannot be laminated at low cost, axisymmetric solenoids are commonly made of solid steel.

The magnetic force produced by a solenoid actuator usually varies considerably with airgap and with coil current. Assuming for illustrative purposes that the steel permeability is infinite (and thus the MMF drop in the steel is zero) and that the two airgaps each have length g and poles of equal area, Ampere's law gives the following formula for H in both airgaps:

$$H = NI/(2g) \tag{7.1}$$

and thus the flux density in both airgaps is:

$$B = \mu_o NI/(2g) \tag{7.2}$$

The normal (perpendicular) magnetic pressure from Maxwell's stress tensor of Chapter 5 is equal to the flux density squared divided by twice the permeability of air. Assuming that the two pole surface "seen" areas are each the same S, then the total magnetic force is:

$$F = (\mu_o NI)^2(2S)/(4g^2 2\mu_o) = \mu_o N^2 I^2 S/4g^2 \tag{7.3}$$

Note that this approximate inherent magnetic force is inversely proportional to the square of the airgap, and thus varies tremendously with airgap. It is also proportional to the square of the coil current, and thus increases greatly with increasing current. When this force is plotted versus x (armature position), a *pull curve* is produced. A set of pull curves for various currents on one plot is often used by actuator designers and users, as will be shown in Example 7.1 and in Chapter 15.

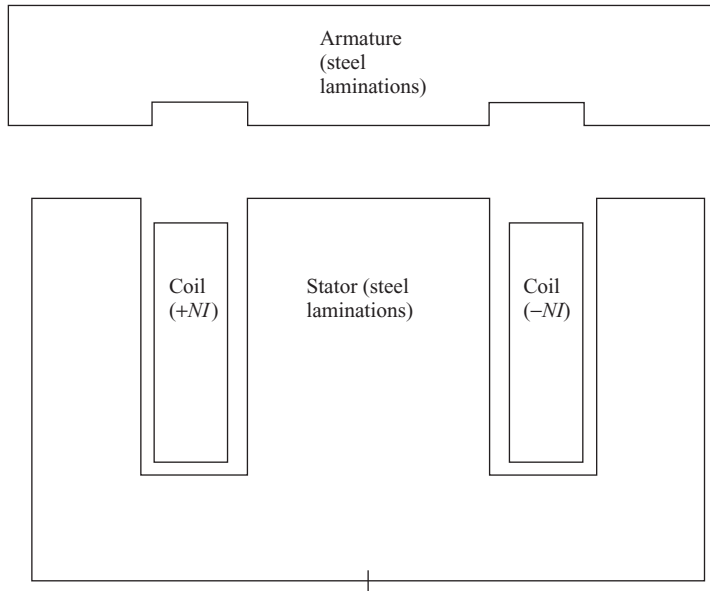

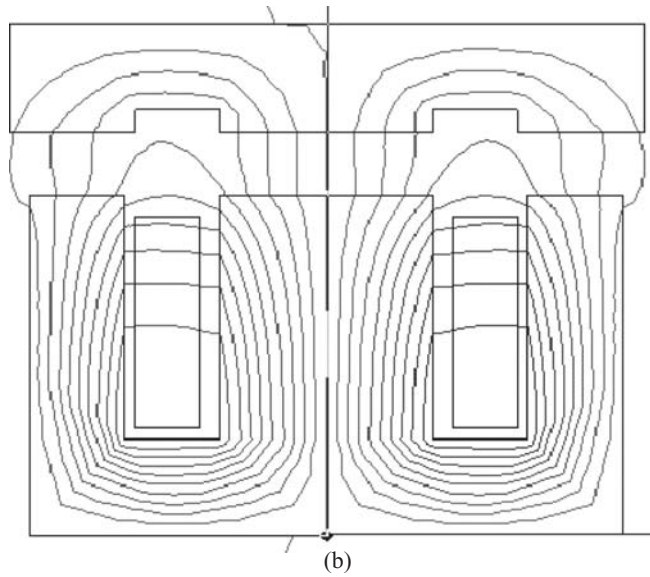

FIGURE 7.1 Typical clapper-type solenoid actuator. (a) geometry, where steel is made up of thin laminations lying in the plane of the page and stacked in the direction out of the page, (b) computer display of flux lines obtained by finite-element analysis.

In reality, due to actual steel B–H curves and complex shapes of steel and air, most solenoid actuators have pull curves that do not closely follow (7.3). For most solenoid actuators, the pull curves are indeed curves, that is, the force varies nonlinearly with both the airgap and the current.

Example 7.1 Fluxes and Forces on Clapper Armature Solenoid of Planar Geometry Figure E7.1.1 shows a planar solenoid with a clapper armature. The stator winding shown has 200 turns and has an end (return) current path not shown outside the core. The dimensions are $w = 10$ mm, $Al_1 = 5$ mm, $Al_2 = 30$ mm, $Al_3 = 5$ mm, $Sl_1 = 15$ mm, $Sl_2 = 30$ mm, $Sl_3 = 15$ mm, and $g = 2$ mm.

(a) Use the reluctance method with steel relative permeability = 2000, assuming no leakage or fringing fluxes, to find the approximate values of the vector **B** and **F** on left side of clapper for $I = 2$ A. Find **F** in newtons per meter depth of the solenoid into the plane of the page.
(b) Repeat (a) to find the vector **B** and **F** on right side of clapper.
(c) Obtain the above answers with finite-element software.
(d) Obtain force F for the above with finite-element software with steel relative permeability = 10,000, and comment on why the results differ from (c).

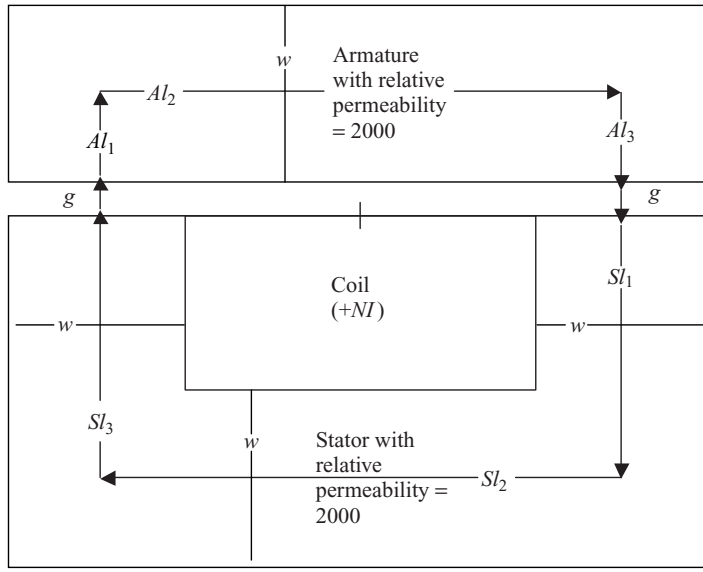

FIGURE E7.1.1 Example 7.1 clapper solenoid actuator of planar geometry.

(e) Repeat (d) for the gap varying from 4 mm to 0.5 mm in 0.5 mm increments and the current varying from 2 to 4 A in 1 A increments.

Solution

(a) The total reluctance is the sum of the stator reluctance $\mathscr{R}_s$, the left airgap reluctance $\mathscr{R}_{gL}$, the armature reluctance $\mathscr{R}_a$, and the right airgap reluctance $\mathscr{R}_{gR}$. Finding each from length over (permeability times area) gives:

$$\begin{aligned}
\mathscr{R}_s &= (Sl_1 + Sl_2 + Sl_3)/[(2000 \times 12.57\text{E}{-7})(w \times 1)] \\
&= (0.06)/(25.14\text{E}{-6}) = 2387 \\
\mathscr{R}_{gL} &= g/[(12.57\text{E}{-7})(w \times 1)] = (0.002)/(12.57\text{E}{-9}) = 159{,}109 \\
\mathscr{R}_a &= (Al_1 + Al_2 + Al_3)/[(2000 \times 12.57\text{E}{-7})(w \times 1)] \\
&= (0.040)/(25.14\text{E}{-6}) = 1591 \\
\mathscr{R}_{gR} &= g/[(12.57\text{E}{-7})(w \times 1)] = (0.002)/(12.57\text{E}{-9}) = 159{,}109
\end{aligned}$$

The flux is then *NI*/(total reluctance) = (200 × 2)/(322,196) = 1.2415E−3 Wb. The flux density in each airgap (and in most of the steel) is the flux divided by ($w \times 1$) = 0.12415 T. From the right-hand rule, the direction of **B** in the left gap is in the –*y* direction. The pressure on each airgap is thus $B^2/(2 \times 12.57\text{E}{-7}) = 6131$ Pa, which when multiplied by the airgap area of 0.01 m^2 gives the force on the left gap = 61.31 N. The force is always attractive, and thus the armature force is in the –*y* direction.

(b) By symmetry, **B** is reversed in direction but force **F** is the same on the right side of the clapper. Thus the total force by the reluctance method is 122.62 N. For a solenoid depth of *d* meters into the page, the force must be multiplied by *d*.

(c) For the airgap shown of 2 mm, a model was quickly made using Maxwell from Ansys, with modeling steps for magnetostatics described in previous chapters. The computed force on the armature for $I = 2$ A is 135.97 N/m depth. This is larger than the force estimated by the reluctance method, partly because the reluctance method does not account for fringing near the poles.

(d) The higher permeability raises the Maxwell computed force to 143.33 N. The small increase is due to the fact that the steel reluctance is small compared with the airgap reluctance for the 2 mm gap.

(e) The force curves obtained using Maxwell's parametric capability are shown in Figure E7.1.2. These pull curves show that the force is highly nonlinear (even for the assumed linear steel *B–H* curve of constant permeability), increasing greatly with small gap and high current.

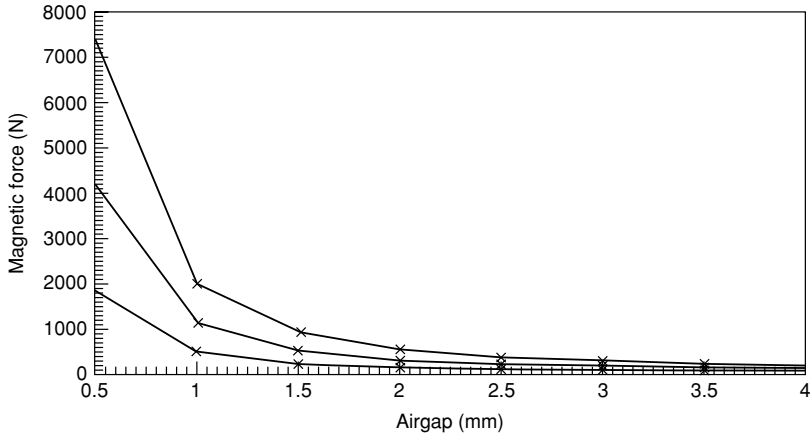

FIGURE E7.1.2 Pull curves computed for Example 7.1. The curves are for currents of 2, 3, and 4 A in order from the lowest curve to the highest curve. The force (N) on the vertical axis is plotted against the airgap (mm) on the horizontal axis.

Example 7.2 Fluxes and Forces on Clapper Armature Solenoid of Axisymmetric Geometry Figure E7.2.1 shows an axisymmetric solenoid with a clapper armature. The number of turns $N = 2000$ and the current $I = 1$ A. The dimensions are $g = 2$ mm, $w_a = 8$ mm, $R_1 = 15$ mm, $R_2 = 25$ mm, $R_3 = 30$ mm, $Z_1 = 8$ mm, and $Z_2 = 23$ mm.

Use the reluctance method with steel relative permeability = 2000, assuming no leakage or fringing fluxes, to find the approximate values of the following.

(a) **B** and **F** on inside of clapper,

(b) **B** and **F** on outside of clapper.

(c) Obtain the above answers with finite-element software.

(d) Obtain the answers for the above with finite-element software with steel relative permeability = 10,000, and comment on why the results differ.

Solution

(a) Path lengths for the reluctance method are seen to be: $Al_1 = 4$ mm, $Al_2 = 20$ mm, $Al_3 = 4$ mm, $Sl_1 = 19$ mm, $Sl_2 = 20$ mm, $Sl_3 = 19$ mm, $w_{si} = 15$ mm, $w_{sa} = 8$ mm, $w_{so} = 5$ mm. The total reluctance is the sum of the stator reluctance $\mathscr{R}_s$, the left airgap reluctance $\mathscr{R}_{gL}$, the armature reluctance $\mathscr{R}_a$, and the right airgap reluctance $\mathscr{R}_{gR}$. Finding each from length divided by the quantity (permeability times area) gives:

$$\mathscr{R}_s = (Sl_1)/\left[(2000 \times 12.57\text{E}{-7})\pi\left(R_3^2 - R_2^2\right)\right] + (Sl_2)/[(2000 \times 12.57\text{E}{-7})\pi(R_1 + R_2)w_{sa}] + (Sl_3)/\left[(2000 \times 12.57\text{E}{-7})\left(\pi R_1^2\right)\right]$$

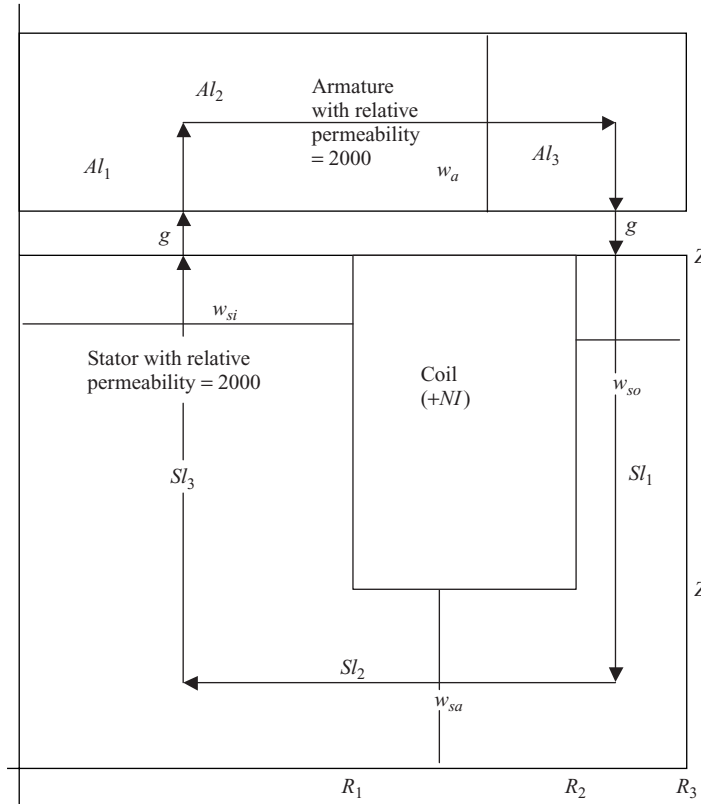

FIGURE E7.2.1 Example 7.2 clapper solenoid actuator of axisymmetric geometry. As customary, the axis of symmetry is the vertical line on the left border.

$$= (0.019)/[(2.514\text{E}{-3})\pi(0.03^2 - 0.025^2)]$$
$$+ (0.02)/[(2.514\text{E}{-3})\pi(0.04)(0.008)]$$
$$+ (0.019)/[(2.514\text{E}{-3})\pi(0.015)^2] = 8748 + 7913 + 10{,}692$$
$$= 27{,}353$$
$$\mathscr{R}_{gL} = g/\left[(12.57\text{E}{-7})\left(\pi R_1^2\right)\right] = (0.002)/[(12.57\text{E}{-7})(\pi 0.015^2)]$$
$$= 2.251\text{E}6$$
$$\mathscr{R}_a = (Al_1 + Al_2 + Al_3)/[(2000 \times 12.57\text{E}{-7})(w_a)\pi(R_1 + R_2)]$$
$$= (0.028)/(2.514\text{E}{-3})(1.\text{E}{-3}) = 11{,}138$$
$$\mathscr{R}_{gR} = g/\left[(12.57\text{E}{-7})\pi\left(R_3^2 - R_2^2\right)\right] = (0.002)/[(12.57\text{E}{-7})(864\text{E}{-6})]$$
$$= 1.842\text{E}6$$

The flux is then NI/(total reluctance) = (2000 × 1)/(4.132E6) = 48.41E–5 Wb. The flux density in the left gap is the flux divided by (πR_1^2) and thus is 0.685 T. The pressure on the left airgap is thus $B^2/(2\times 12.57\text{E}{-7}) = 187\text{E}3$ Pa, which when multiplied by the airgap area of 707E–6 m^2 gives the force on the left gap = 132 N. The flux density in the right gap is the flux divided by $\pi(R_3^2 - R_2^2)$ and thus is 0.56 T. The pressure on the right airgap is thus $B^2/(2 \times 12.57\text{E}{-7}) = 124.7\text{E}3$ Pa, which when multiplied by the airgap area of 864E–6 m^2 gives the force on the left gap = 108 N. The total force is 240 N and is always attractive, and thus the armature force is in the $-z$ direction.

(b) B is about 0.82 T on the inner pole and 0.45 T on the outer pole. $F = 279.41$ N.

(c) The force increases to 285.1 N because of the higher steel permeability.

7.1.2 Plunger Armature

Unlike a clapper armature, a plunger armature is not flat or cupped like a hand, but is basically a brick or cylinder, often shaped like a piece of chalk [3]. Figure 7.2 shows a typical cylindrical plunger actuator in a DC solenoid.

Unlike a clapper armature, where magnetic force in the direction of linear motion is produced both where the flux enters and leaves, the plunger armature has useful magnetic force on only one area. The useful force is produced only at the end of the plunger, which is usually either a flat rectangular or circular area or a conical area. The flux usually leaves this end area, and enters the armature through the sides of the plunger. Little or no useful magnetic force is produced by the flux on the sides of the plunger, and thus the plunger armature solenoid might have less force per unit volume than the clapper armature solenoid of the preceding Section 7.1.1.

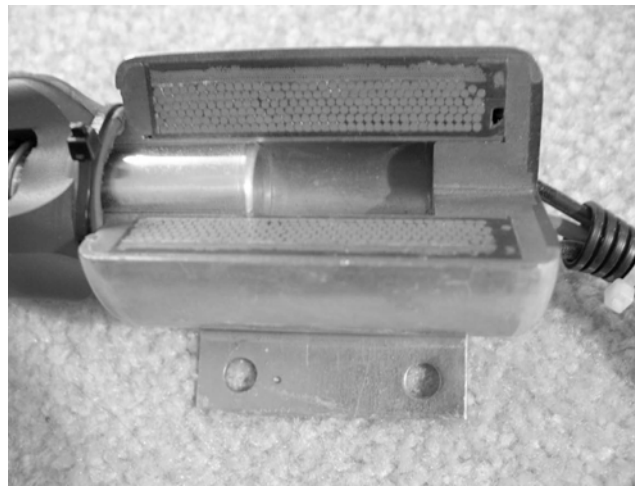

FIGURE 7.2 Photo of typical plunger-type axisymmetric solenoid actuator. A sector of the stator has been sawed away to show the coil cross section.

While the plunger is often a pure cylindrical shape as shown in Figure 7.2, it can also be shaped for "constant force" as the armature moves. Such "constant force" or "proportional" solenoids will be discussed in later sections of this chapter.

If the plunger is cylindrical as in Figure 7.2, then the solenoid is usually axisymmetric, and is thus made of solid steel. However, if the plunger is a rectangular brick shape, then it can be inexpensively laminated and placed in a laminated stator to form a planar solenoid. As mentioned in Chapter 2, eddy currents are reduced when steel is laminated. Reducing eddy currents gives reduced losses and increased magnetic forces, as will be further discussed in Chapters 8 and 9.

Finite-element analysis of axisymmetric plunger armature solenoids has been combined with *design optimization methods* to mathematically obtain optimum designs [4]. Design optimization software has been developed over recent years [5] and is becoming increasingly powerful and available. A simpler way, however, to optimize design of magnetic devices is to run multiple finite element analyses with varying design parameters such as pole width and armature length, and choose the design that produces the highest force. Such multiple runs are called *parametric finite-element analysis.* Design optimization will be further discussed in Chapter 15.

Example 7.3 Fluxes and Forces on Planar Plunger Armature Solenoid Figure E7.3.1 shows a planar solenoid with a plunger armature. The number of turns $N = 1000$ and the current $I = 2$ A. The dimensions are $w = 8$ mm, $g = 4$ mm, $g_s = 1$ mm, $Al_1 = 4$ mm, $Al_2 = 22$ mm, $Sl_1 = 8$ mm, $Sl_2 = 20$ mm, $Sl_3 = 34$ mm, and $Sl_4 = 15$ mm.

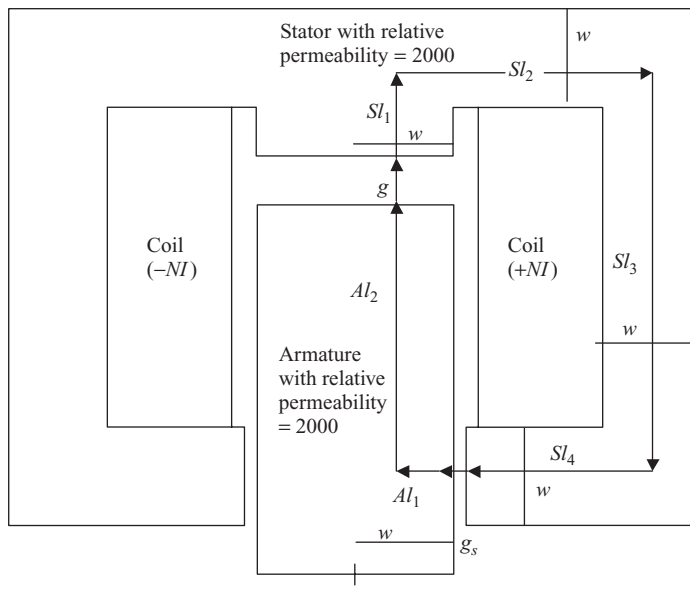

FIGURE E7.3.1 Example 7.3 plunger solenoid actuator of planar geometry.

(a) Use the reluctance method with relative permeability = 2000 in the steel, assuming no leakage flux nor fringing flux, to find the approximate values of **B** and **F** on the end of the plunger.
(b) Compute the above **B** and **F** using finite-element software.
(c) Obtain the answers for the above with finite-element software with steel relative permeability = 10,000, and comment on why the results differ.

Solution

(a) There are two flux paths, left and right, of equal lengths, areas, and reluctances. The total reluctance of the right path is the sum of the stator reluctance $\mathscr{R}_s$, the working airgap reluctance $\mathscr{R}_g$, the armature reluctance $\mathscr{R}_a$, and the side airgap reluctance $\mathscr{R}_{gS}$. Finding each from length over (permeability times area) gives:

$$\begin{aligned}
\mathscr{R}_s &= (Sl_1 + Sl_2 + Sl_3 + Sl_4)/[(2000 \times 12.57\text{E}{-7})(w \times 1)] \\
&= (0.077)/[(2.514\text{E}{-3})(0.008)] = 3829 \\
\mathscr{R}_g &= g/[(12.57\text{E}{-7})(w \times 1)] = (0.004)/(10.06\text{E}{-9}) = 397{,}614 \\
\mathscr{R}_a &= (Al_1 + Al_2)/[(2000 \times 12.57\text{E}{-7})(w \times 1)] \\
&= (0.026)/[(2.514\text{E}{-3})(0.008)] = 1293 \\
\mathscr{R}_{gS} &= g_s/[(12.57\text{E}{-7})(w \times 1)] = (0.001)/(10.06\text{E}{-9}) = 99{,}443
\end{aligned}$$

The right flux is then NI/(total reluctance) = $(1000 \times 2)/(502{,}179)$ = 3.983E–3 Wb. The flux density in the working airgap g (and in most of the steel) is the flux divided by $(w \times 1) = 0.498$ T. From the right-hand rule, the direction of $\boldsymbol{B}$ in the working gap is in the $-y$ direction. The pressure on each airgap is thus $B^2/(2 \times 12.57\text{E}{-7}) = 98{,}582$ Pa, which when multiplied by the total working airgap area of 0.016 m^2 gives the force on the armature = 1577 N (for 1 m depth). The force is always attractive, and thus the armature force is in the y direction. To find the force on the solenoid of depth d meters, the 1577 N must be multiplied by d.
(b) $F = 1863$ N for 1 m depth using Maxwell, and B at the plunger end varies around approximately 0.51 T.
(c) $F = 1900$ N/m depth using Maxwell, higher because of the higher steel permeability.

Example 7.4 Fluxes and Forces on Axisymmetric Plunger Armature Solenoid Figure E7.4.1 shows an axisymmetric solenoid with a plunger armature. The number of turns $N = 400$ and the current $I = 4$ A. The dimensions are plunger and pole outer radius $R_P = 20$ mm, side airgap outer radius $R_{PG} = 22$ mm, stator yoke outer radius

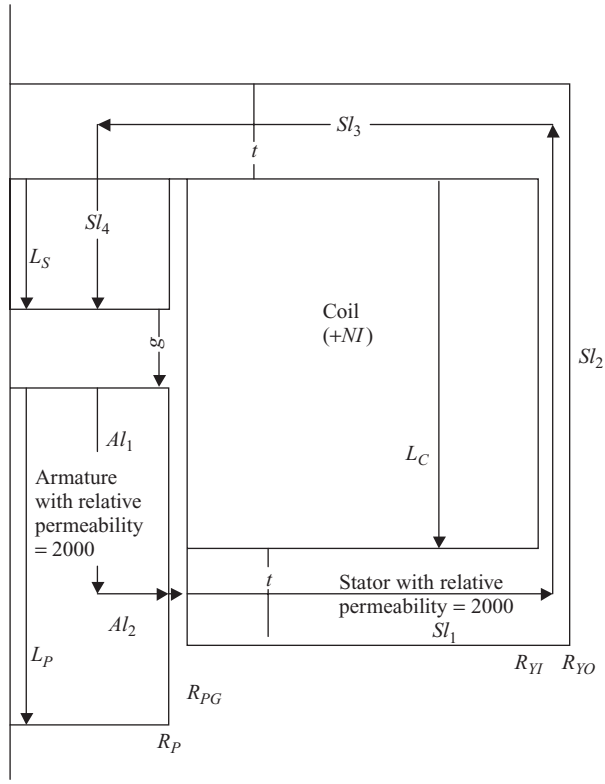

FIGURE E7.4.1 Example 7.4 plunger solenoid actuator of axisymmetric geometry.

$R_{YO} = 70$ mm, stator yoke inner radius $R_{YI} = 66$ mm, working airgap $g = 10$ mm, plunger length $L_P = 42$ mm, stator stopper length $L_S = 16$ mm, coil axial length $L_C = 46$ mm, and stator yoke axial thickness $t = 12$ mm (on top; same on bottom).

(a) Use the reluctance method, assuming no leakage flux, to find the approximate values of **B** and **F** in the working airgap on the end of the plunger with steel relative permeability = 2000.

(b) Compute the above **B** and **F** using finite-element software.

(c) Obtain the answers for the above with finite-element software with steel relative permeability = 10,000, and comment on why the results differ.

Solution

(a) The total reluctance is the sum of the stator reluctance $\mathscr{R}_s$, the working airgap reluctance $\mathscr{R}_{gW}$, the armature reluctance $\mathscr{R}_a$, and the side airgap reluctance

$\mathcal{R}_{gS}$. Each is found from length over permeability times area, where the areas are the average areas. The reluctances are then:

$$\begin{aligned}
\mathcal{R}_s &= (Sl_1 + Sl_3)/[(2000 \times 12.57\text{E}{-7})[t \times \pi(R_{PG} + R_{YI})] \\
&\quad + (Sl_2)/[(2000) \times 12.57\text{E}{-7})(\pi(R_P^2 - R_{YI}^2)] \\
&\quad + (Sl_4)/[(2000) \times 12.57\text{E}{-7})(\pi R_P^2)] \\
&= (0.046 + 0.058)/[2.514\text{E}{-3} \times 0.012 \times \pi(0.022 + 0.066)] \\
&\quad + (0.046 + 0.012)/[2.514\text{E}{-3} \times \pi(0.07^2 - 0.066^2)] \\
&\quad + (0.016 + 0.006)/[2.514\text{E}{-3}(\pi 0.02^2)] \\
&= 12{,}470 + 13{,}500 + 6964 = 32{,}934 \\
\mathcal{R}_{gW} &= g/[(12.57\text{E}{-7})(\pi R_P^2)] = 6.3307\text{E}6 \\
\mathcal{R}_a &= (Al_1)/[(2000) \times 12.57\text{E}{-7})(\pi R_P^2)] \\
&\quad + (Al_2)/[(2000 \times 12.57\text{E}{-7})[t \times \pi(R_P)] \\
&= (0.026)/[2.514\text{E}{-3} \times \pi 0.022)] \\
&\quad + (0.01)/[2.514\text{E}{-3} \times 0.012 \times \pi 0.02] = 8230 + 5276 \\
&= 13{,}506 \\
\mathcal{R}_{gS} &= (R_{PG} - R_P)/[(12.57\text{E}{-7})(2\pi R_P t)] = 1.055\text{E}6
\end{aligned}$$

The flux is then NI/(total reluctance) = 1600/(7.426E6) = 215.5E–6 Wb. The flux density in the working airgap (and in most of the steel) is the flux divided by $(\pi R_P^2) = 0.1715$ T. From the right-hand rule, the direction of **B** in the left gap is in the $-z$ direction. The pressure on the working airgap is thus $B^2/(2 \times 12.57\text{E}{-7}) = 11{,}694$ Pa, which when multiplied by the airgap area of (πR_P^2) square meters gives the force = 14.7 N. The force is always attractive, and thus the armature force is in the $+z$ direction.

(b) The computed $F = 19.34$ N using Maxwell. The airgap B on the end of the plunger is approximately 0.170 T.

(c) The computed F using Maxwell is now 19.66 N, with airgap $B = 0.174$ T. These are both raised because of the higher steel permeability.

7.2 VOICE COIL ACTUATORS

Instead of forces on steel, Lorentz force on current-carrying coils is used in many actuators. They are called *voice coil actuators* because of their common use in loudspeakers.

From the Lorentz force equation of Chapter 5, the force on an N-turn coil of average turn length l is:

$$F = NBIl \tag{7.4}$$

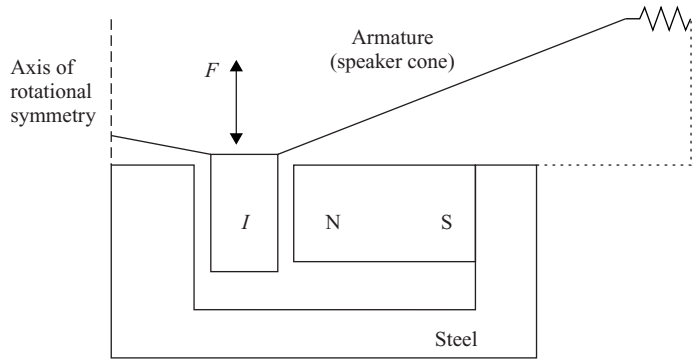

FIGURE 7.3 Typical voice coil actuator, shown driving a loudspeaker. The movable voice coil carries the current I and is subjected to the magnetic field from a permanent magnet with north (N) and south (S) poles.

where B is the magnetic flux density perpendicular to the coil direction and F is perpendicular to both B and the coil direction. The directions follow the right-hand rule as shown in Figure 7.3 for a typical voice coil in a loudspeaker. Note that when the current direction is reversed, then (assuming that the direction of B is unchanged) the direction of the force is reversed. The reversible force of a voice coil actuator is an advantage over the force of moving iron actuators of the preceding sections, which is directed to attract the iron armature toward the iron stator regardless of the direction of the current. Another advantage over solenoid actuators is that voice coil force is much more independent of armature position and is proportional to current. A minor disadvantage is that the voice coil current must be supplied via a flexible lead, and thus the proper stranded wire must be selected for reliable long-term operation.

Because coils are most easily wound on cylindrical bobbins, voice coil actuators often have axisymmetric geometry. No laminations are needed because the magnetic flux density B is constant and is almost always produced by a permanent magnet. There is some B produced by the voice coil current, but it is usually negligibly small compared to the B produced by the permanent magnet. An advantage of permanent magnets is that their B is produced without any current or associated power loss and temperature rise.

Besides loudspeakers, another very popular use of voice coil actuators for DC (not AC) operation is for computer disk drive head actuation. The current applied is a DC step or pulse to position the voice coil armature at the desired radius (track) on the disk. Often the coil is on a pivot, like old-fashioned turntable arms, as shown previously in Figure 1.3 of Chapter 1. Each of the two radial sectors of the coil is subjected to a permanent magnet field. The field direction is upward in one sector and downward in the other, and since the current direction is opposite in the two coil sectors, their Lorentz forces add to produce a torque on the coil, as shown in Figure 7.4. Note that the force F on each coil remains in the same x direction as long as the coil moves for a "short stroke" of less than about half of the *pole pitch p.* If the motion is not limited to much less than the pole pitch, then for the force (and/or torque) to remain

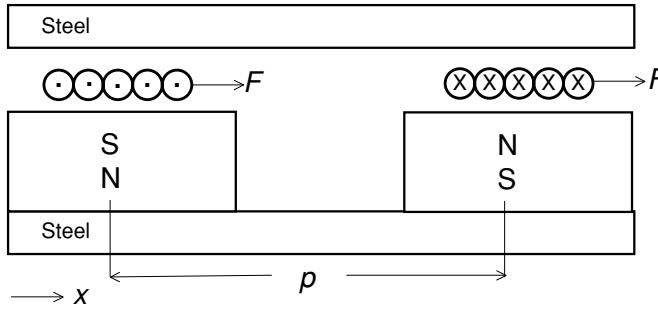

FIGURE 7.4 Cross section of disk drive actuator of Figure 1.3, showing forces F on both halves of the coil that positions the heads.

in the same x direction, the current in the coils must be *commutated*, that is, switched in direction. Thus permanent magnet motors with continuous unlimited motion are commutated either electronically or by mechanical switching via brushes. This book is devoted to actuators and sensors of limited motion with no commutation.

The time to move the coil arm to the desired position is called *seek time* and should be as small as possible to enable high speed data access for computation [6]. Because voice coils are made of copper or aluminum, both of which are lighter than steel or iron, voice coil actuators are preferred over moving iron solenoid actuators for disk head operation. Also, because voice coil force is proportional to current and is relatively independent of position, feedback control based on linear systems can be readily applied.

Example 7.5 Force of Voice Coil Actuator A voice coil has a resistance of 20 Ω and 400 turns. A permanent magnet provides a DC magnetic flux density of 0.8 T in the radial r direction. The average radius r of the voice coil is 15 mm. Given 12 V DC applied to the voice coil, find the steady-state force produced.

Solution From Ohm's law, the DC current $I = 12/20 = 0.6$ A. The average length of a coil turn is 2π times the average radius $= 0.015$ m, giving $l = 0.0942$ m. Thus the desired $F = 400(0.8)(0.6)(0.0942) = 18.1$ N.

7.3 OTHER ACTUATORS USING COILS AND PERMANENT MAGNETS

Besides solenoid and voice coil actuators, other actuators are available that use both permanent magnets and coils. The advantage of using permanent magnets is that the **B** they produce does not require current or power loss that coils do. The **B** of the permanent magnets interacts with the **B** of coils to produce the force. In some cases the permanent magnets produce *latching force* to hold the armature in a certain latched condition without requiring any input current.

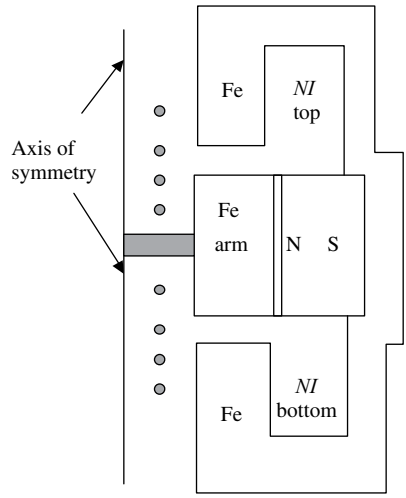

FIGURE 7.5 Actuator with both permanent magnet and coils in stator. The armature labeled "arm" moves either up or down.

Many different designs are possible. Figure 7.5 shows a design from a paper by Lequesne [7]. It is a long-stroke actuator with one radially magnetized permanent magnet, a steel or iron armature, and two coils. The coils are wound and connected so that they both carry current in the same direction. For example, if they both carry current out of the page, then the lower pole of the moving iron armature has higher flux than the upper pole, and the armature experiences a downward force. Reversal of the current gives an upward force, and no current gives zero (balanced) force on the armature. Thus the armature experiences bidirectional force. The force varies with position due to the changing of both airgaps.

Other possible designs include the tubular linear actuator of Figure 1.5, where the stator contains permanent magnets. In some actuators the armatures are permanent magnets [8, 9], but the design must carefully avoid breakage of the fairly brittle permanent magnet material. Besides permanent magnets, materials that are magnetostrictive are occasionally used in actuators, but are more often used in sensors as will be described in Chapter 11.

7.4 PROPORTIONAL ACTUATORS

In many applications, proportional actuation is desired. Such actuation ideally produces a position x that is directly proportional to current or voltage, for example:

$$x = kI \tag{7.5}$$

where k is the proportionality constant. Note that x is independent of inertia, load forces, and other external forces. Such ideal proportional positioning is highly desired for valve operation and other applications.

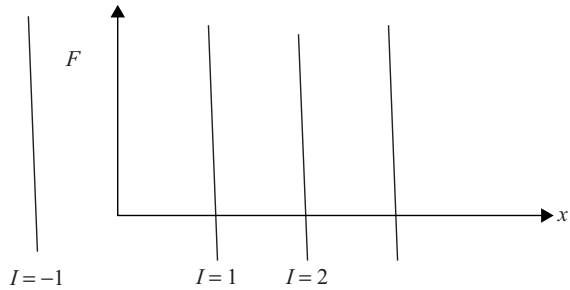

FIGURE 7.6 Ideal proportional actuator force.

A graphical depiction of proportional actuation is shown in Figure 7.6. It shows force F as a function of x and I for both positive and negative currents I. Note that the slopes for all currents I are ideally infinite, that is, the lines are vertical and indicate no effect of external force.

In the real world, infinite slopes are not possible. Instead, a fairly high value of negative slope can be obtained by use of a mechanical spring. Figure 7.7 shows that the combination of a spring that produces a spring force:

$$F_s = k_x x \tag{7.6}$$

along with a magnetic actuator that produces a force F_{mag} that is independent of x and proportional to I, obtains a total force F that approximates the desired set of proportional force lines. Note that the bigger the spring constant, the steeper are the total force lines, which is desirable. However, the bigger the spring, the larger is the magnetic force required for a specified total force, since the spring and magnetic forces are in opposition.

The required magnetic force that is independent of x and proportional to I is produced by what is commonly called a *constant force magnetic actuator.* From the

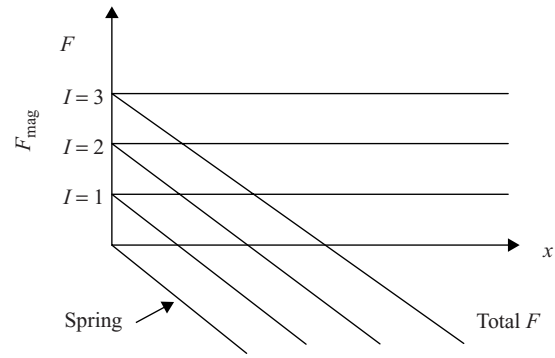

FIGURE 7.7 Nonideal proportional actuator produced by constant magnetic force and opposing spring force.

various types of magnetic actuators discussed in preceding sections, the type that inherently provides constant force is the voice coil actuator.

However, solenoid actuators can also be specially designed for proportional actuation. Without special design, solenoid actuators tend to produce force that varies greatly with position according to (7.3). To obtain force that is independent of position and proportional to current, much design work is required, usually involving electromagnetic finite-element analysis of various possible shapes of steel armatures and pole pieces. With such design work, the magnetic force can be made approximately "constant", that is, independent of position x over a fairly large variation of x. Some nonconstant regions, called *deadbands*, are present and must be avoided during operation. Figure 7.8 shows a typical design of a "constant force" plunger-type solenoid actuator. As pointed out by Lequesne [10], the plunger is usually conical (not cylindrical), and the stator poles usually are angled as well. The exact angles and shapes must be carefully computed using finite-element software or (with less certainty) reluctance methods. Also, steel saturation must occur at the proper level to produce a force that is proportional not to the current square of equation (7.3) but to the first power of current.

Since steady-state current (from Ohm's law) is V/R, a proportional actuator also has steady-state position proportional to applied voltage. Thus proportional actuators can be readily controlled by linear feedback control systems.

The lowest cost way to vary applied voltage is to use a chopper circuit to obtain *pulse–width modulation (PWM).* A given DC voltage, such as battery voltage in an automobile, is switched on and off. Figure 7.9 shows a typical PWM voltage waveform. In this case the battery voltage is 24 V and the switching frequency is 1 kHz. Also in the figure, the "duty cycle" is approximately 33%, that is, that the

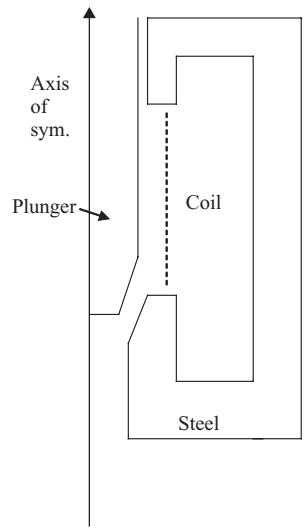

FIGURE 7.8 Plunger solenoid shaped for approximately constant force.

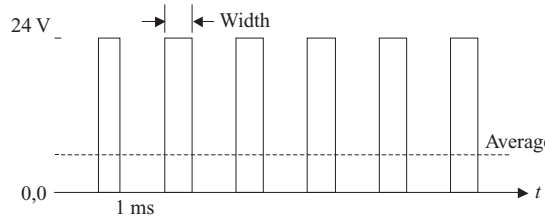

FIGURE 7.9 Typical PWM voltage waveform.

voltage is "on" about one-third of the time. The average, or DC, voltage, equals duty cycle times battery voltage, and thus is 8 V in this case.

The choice of switching frequency f involves trade-offs. Its period, $T = (1/f)$ should be much faster than the desired actuation time, yet not so high as to produce significant eddy currents. The switching frequency produces corresponding pulses in magnetic force, which is not necessarily bad. The force pulsations, called *dither*, can often help overcome static friction, often called *stiction*.

7.5 ROTARY ACTUATORS

Many applications need rotary motion, that is, motion along a circular arc instead of the straight line of linear actuators. Rotary actuators are also sometimes called *torquers*, because they produce torque. This book is restricted to limited motion, and thus rotary actuators or torquers are studied, but not electric motors in general, because they produce motion that is many times 360°/min.

Rotary magnetic actuators are used at times in electrohydraulic servo valves and in computer disk drives. As mentioned in Section 7.3, voice coil actuators in disk drives sometimes operate on a pivoted arm, thus producing rotary motion.

The most common rotary magnetic actuator is the *step motor*. It is also called a *stepper motor* or *stepping motor*.

Step motors get their name because they provide rotary motion in incremental steps. They are very popular because their incremental motion is easily controlled by microprocessors or other digital devices that produce digital pulses, that is, steps of DC current.

Figure 7.10a shows one quadrant of a typical step motor. Like most step motors, the rotor (armature) is on the inside and is made up solely of steel laminations. Over all four quadrants, the rotor shown here has 8 teeth, and the outer stator has 12 teeth. When a step of current is applied to the proper stator winding, the rotor wants to align its teeth for minimum reluctance for the flux of that winding. Hence they are also called *variable reluctance motors*. Thus Figure 7.10b shows that for flux produced by current in the stator slots at approximately 20° and 70°, the rotor tends to move to the position shown. For highest torque, the airgap between stator and rotor is usually quite small, on the order of 0.1 mm. For the 12 stator teeth and 8 rotor teeth shown, each step (increment) in motion is (360/8)–(360/12) = 15°. Other numbers

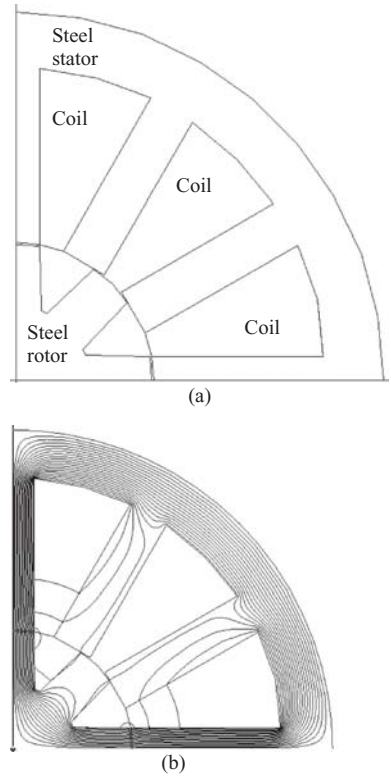

FIGURE 7.10 Typical step motor. (a) geometry of one quadrant, (b) Computer display of calculated flux lines.

of teeth can be chosen, but the rotor and stator must never have the same number of teeth.

Step motors can also be operated continuously, that is, over multiple revolutions. Under continuous operation they are commonly called *switched reluctance motors.* Again their advantage is the simple rotor construction, requiring only steel laminations and no coil or permanent magnet.

Another rotary actuator with a rotor made only of steel is shown in Figure 7.11. Its stator has a solenoidal coil embedded in steel that provides three-dimensional (3D) flux paths. The design shown in Figure 7.11 has been used by Sandia National Laboratories [11] and has four teeth on both the stator and the rotor. Its maximum rotation with four poles is less than 90°. Its flux paths and torques have been computed by 3D finite-element analysis [11]. Many design variations are possible.

Rotary actuators and motors are often used to drive gears that convert their motion to straight-line motion. Gears commonly used include ball screws and rack-and-pinions. However, as mentioned in Chapter 1, a linear (straight line) actuator has the advantages of reduced maintenance, reduced friction, and longer life.

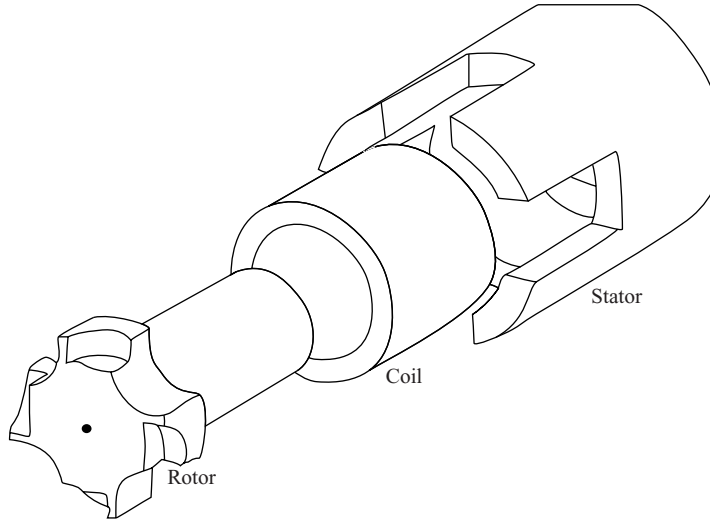

FIGURE 7.11 Rotary actuator with solenoidal winding and three-dimensional flux paths.

7.6 MAGNETIC BEARINGS AND COUPLINGS

Moving objects require bearings, and *magnetic bearings* feature long life due to their avoidance of mechanical wear. Magnetic bearings are a type of magnetic actuator designed to suspend a rotating axle with no mechanical contact. Benefits include higher reliability with little or no maintenance, reduced frictional losses, no contaminating or flammable lubricants, reduced machine vibration, and improved monitoring and diagnostics. Recent advances in magnetic bearing technology, including miniaturization, simplicity, and integration have overcome many of these limitations [12].

Figure 7.12 shows the basic layout of a typical active magnetic bearing system. Stationary electromagnets are positioned around the rotating machine. Typically, two radial magnetic bearings are used to support and position the shaft in the radial directions and one thrust bearing is used to support and position the shaft along the longitudinal (axial) direction. A shaft that is completely supported by magnetic bearings is said to provide support along five axes because the bearings react to motion along the three translational axes and two angular axes. Ideally, the magnetic bearing offers no rotational resistance.

An active magnetic bearing consists of a stator containing the electromagnets and position sensors, and the rotor, which rotates with the shaft. During operation, each magnetic bearing rotor is ideally centered in the corresponding stator so that contact does not occur. The position of the shaft is controlled using a closed-loop feedback system. The position sensors detect the local displacements from the shaft, and these signals are sent to a digital controller. The controller processes these signals and computes how to redistribute the currents in the electromagnets to restore the shaft

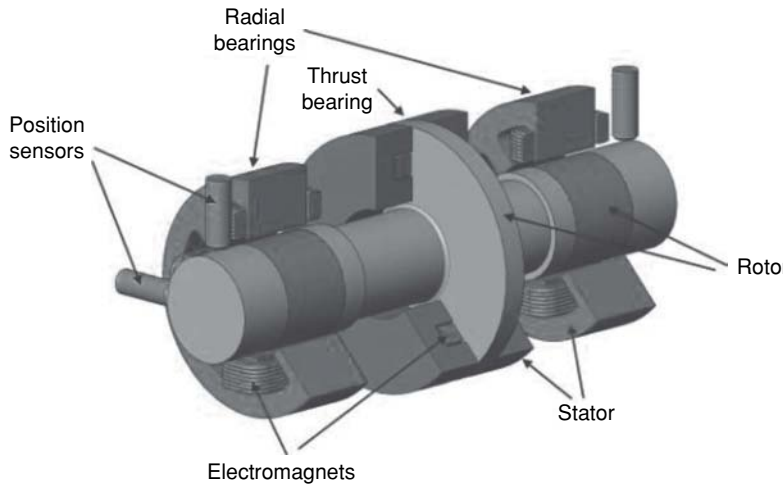

FIGURE 7.12 Magnetic bearing basic layout. Used by permission of Synchrony [12].

to its centered position. Amplifiers in the controller then readjust the currents in the electromagnets accordingly, typically 15,000 times per second.

Like other kinds of bearings, magnetic bearings provide stiffness and damping. However, unlike other bearings, magnetic stiffness and damping vary as a function of disturbance frequency. It is often convenient to model the bearing as a transfer function with an amplitude and phase that vary with frequency. The optimization of this transfer function is a critical step in ensuring that the magnetic bearing performance has adequate stability and force rejection capability over a range of frequencies. The stiffness and damping can be optimized by simply changing the control algorithm.

The load capacity of a radial bearing is the product of the rotor circumference, the active length, and the equivalent bearing pressure. Because the bearing pressure of a magnetic bearing is limited to below 20 bar from Figure 5.7, many times less than the bearing pressure of oil-lubricated fluid film bearings, the size will in general be greater for the same load capacity. Also, the end windings and position sensors increase the length of the magnetic bearing beyond its active length.

Through recent design innovations, the size of radial magnetic bearings has been reduced by more than 30% [12]. The bearing pressure for radial bearings has been improved by increasing the amount of electrical steel at the bore of the stator where the force is created. At the same time, the outer circumference of the stator has been reduced by splitting the flux paths and isolating the electromagnets. Finally, the length of the radial magnetic bearing has been reduced by developing position sensors that can be integrated into the electromagnets.

The controller for magnetic bearings has recently been miniaturized. The position sensing uses frequency modulation to produce a digital counter. A processor handles network communications, performs digital processing, and generates timing

FIGURE 7.13 Fusion® magnetic radial and thrust bearings with integrated control electronics. The radial bearing has a load capacity of 1330 N, and the thrust bearing has a load capacity of 4448 N. Used by permission of Synchrony [12].

signals for the amplifiers. The controller is now often small enough to be completely integrated into the magnetic bearing. The short distance from the controller to the magnetic coils means that EMI (to be discussed in Chapter 13) is greatly reduced. Typically the controller is supplied with a DC voltage between 48 and 300 V, and each coil magnet has a dedicated power amplifier designed to supply its power factor that is lagging due to its inductance.

The "health" of bearings is important to prevent failure, and can easily be monitored with magnetic bearings. Their built-in position sensors monitor shaft position and activate alarms if vibrations grow too large. Adding up all these advantages, magnetic bearings often outshine mechanical bearings in performance and price.

Figure 7.13 shows magnetic bearings with built-in controllers. These bearings are now smaller than past magnetic bearings that required a large external controller [13]. Each bearing is powered with 48 V DC and includes a dedicated Ethernet port for high speed communications and health monitoring. The small size and simplified mechanical and electrical interface makes it very easy to integrate the bearing into rotating machines such as motors, pumps, fans, and turbines [12].

Instead of the electromagnets of Figures 7.12 and 7.13, some magnetic bearings use permanent magnets [14]. Permanent magnet bearings developed at the Lawrence Livermore National Laboratory [15] are called *passive* because their permanent magnets levitate the rotating member without electromagnets. Such passive bearings do,

however, require special passive *stabilizers* to overcome the inherent instability of interacting permanent magnets that was predicted in 1842 by Samuel Earnshaw. One type of stabilizer [15] uses Halbach magnet arrays as discussed in Chapter 5.

Some magnetic bearings also serve as *magnetic couplings*, which transfer torque between two rotating members through seals and walls without mechanical contact [16]. Magnetic couplings can greatly reduce undesirable transfer of vibration and noise. The couplings can be either synchronous (maintaining the identical speed for both rotating members) or asynchronous with the driven member having a different speed. Asynchronous eddy current couplings produce reduced speed and have the disadvantage of high power loss compared to synchronous couplings.

Also required for many rotating systems are magnetic brakes and clutches, which are often operated by clapper armature solenoids [17,18]. So-called *magnetic particle* brakes and clutches contain ferromagnetic particles, which experience forces as explained in Section 5.8.

7.7 MAGNETIC SEPARATORS

Another type of actuator using permanent magnets and/or coils is the *magnetic separator*. Its stator produces magnetic force on multiple "armatures" consisting of ferromagnetic particles of various sizes and shapes. A practical way to calculate the force acting on small ferromagnetic particles is to use the equations for force per unit volume derived previously in Section 5.8.

In applications in the mining and recycling industries, a fluid (air, other gas, or liquid) containing both nonmagnetic and magnetic objects is fed to a magnetic separator. The fluid can sometimes have enough ferrous particles to be considered a *ferrofluid* [19]. The separator has permanent magnets and/or coils carrying either conventional or superconducting current, and is used to separate out the magnetic objects or particles, often by their attraction to steel wires [20].

Example 7.6 Separator Using a Steel Wire The classic paper by Oberteuffer [20] examines magnetic separation forces due to cylindrical ferromagnetic wires placed in a uniform DC magnetic field. A typical wire and large particle are shown in Figure E7.6.1. Use finite-element software to compute the magnetic flux lines of the figure, and then (using the equations of Section 5.8 in the software) compute the magnetic force for the particle diameters 0.1, 1.0, 2.0, and 3.0 μm. Compare the computed forces for both cylindrical and spherical particles with results computed using simplified equations derived by Oberteuffer [20].

Solution Rather than sketch by hand the magnetic flux lines as in Figure 4 of Oberteuffer [20], in Figure E7.6.1 the flux lines have been computed using the finite-element software Maxwell. The relative permeability of both the wire and the particle is assumed to be 1000, that is $\mu_{rp} = 1000$. Since Figure E7.6.1 is a 2D planar analysis, the particle (like the wire) is assumed to be a cylinder normal to the paper. Note that, as

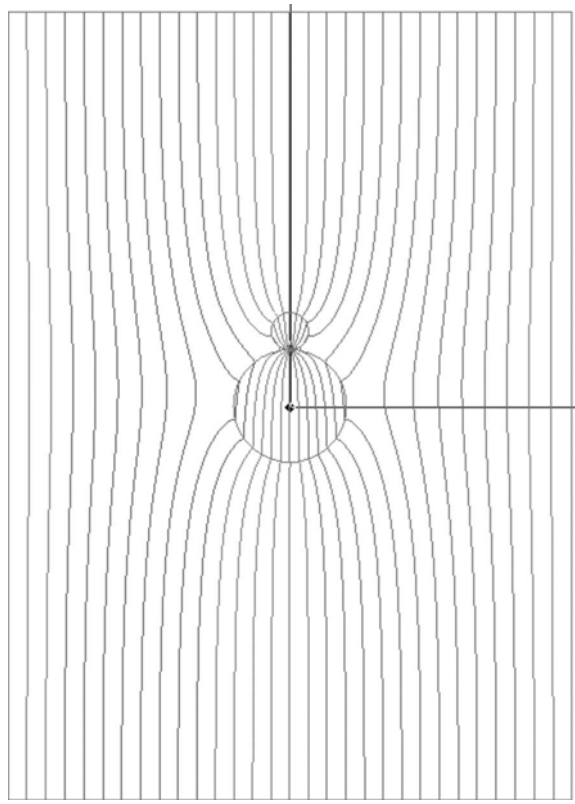

FIGURE E7.6.1 Ferromagnetic wire of radius 10 μm below a ferromagnetic particle of radius 3.3 μm, with flux lines computed by finite-element software. Similar to Oberteuffer [20], both objects are immersed in a uniform magnetic field. Here the field is assumed to be $\mathbf{B} = 1$ T in the vertical y direction outside the modeled region of size 100 by 140 μm.

might be expected, the flux pattern is not symmetric above and below the wire because the large particle alters the field. Unfortunately, Oberteuffer's derived formulas do not account for such alteration by the particle; they only include the alteration of the field by the wire itself. Also, his formulas assume that the magnetic flux density at the *center* of the particle acts on the entire particle.

Based on the above assumptions, Oberteuffer derives a formula for the vertical magnetic force on the particle of Figure E7.6.1 which can be written as [20]:

$$F_{my} = -2v_p \left(1 - \frac{1}{\mu_{rp}}\right)\left(H_0 + H_0\frac{a^2}{r^2}\right) B_0 \frac{a^2}{r^3} \tag{E7.6.1}$$

where v_p is the volume of the particle of relative permeability μ_{rp} located at radius r from the center of the wire of radius a in a y-directed magnetic field in air of intensity

H_0 and flux density B_0. Dividing both sides of (E7.6.1) by volume v_p, one obtains the *force density* expression:

$$f_{my} = -2\left(1 - \frac{1}{\mu_{rp}}\right)\frac{B_0}{\mu_0}\left(1 + \frac{a^2}{r^2}\right)B_0\frac{a^2}{r^3} \tag{E7.6.2}$$

which is in units of N/m^3 and shall be called the Oberteuffer force density from now on.

To compare Oberteuffer's approximate force density (E7.6.2) with finite-element computations using (5.32) of Section 5.8, the geometry of Figure E7.6.1 is here examined for the case $B_0 = 1$ T. The relative permeability μ_{rp} of both the particle and the wire is assumed to be 1000. Various particles are considered, but all particles are assumed centered at radius 13.3 μm from the center of the wire as shown in Figure E7.6.1. Substituting $r = 13.3\text{E}{-6}$ and $a = 10.\text{E}{-6}$ in (E7.6.2) along with $B_0 = 1$ and $\mu_{rp} = 1000$ and $\mu_0 = 12.57\text{E}{-7}$ obtains $f_{my} = -105.75\text{E}9$ N/m^3.

Finite-element force computations using (5.34) and the model of Figure E7.6.1 were carried out as follows. The flux density B needed for (5.34) was computed using the particle permeability changed to that of air, and then a postprocessor calculator macro was developed for Maxwell to carry out the operation of (5.34) to compute and display the force density. A typical display of force density is shown in Figure E7.6.2, which is available in color on the internet but shown in black and white in print [21].

To find the total force acting on a ferromagnetic particle, the volume integrals of Section 5.8 can be carried out. Both the integrals of (5.38) and Problem 5.15 are

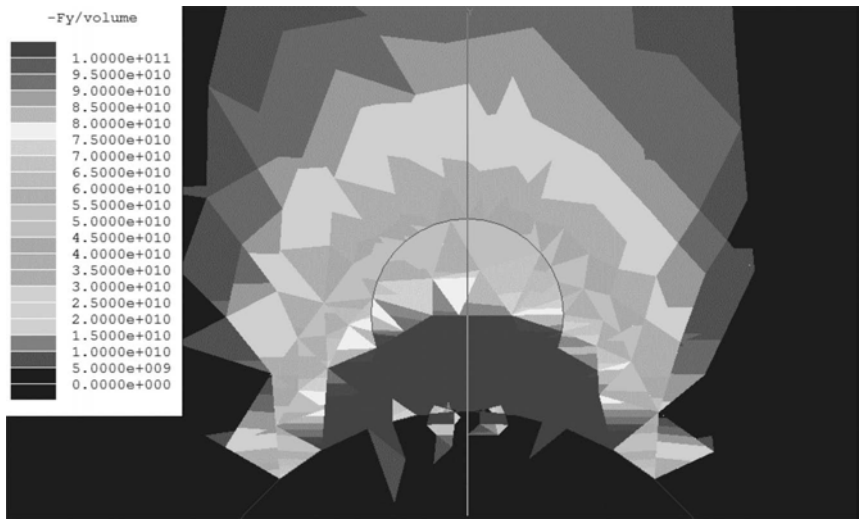

FIGURE E7.6.2 Zoomed plot of geometry of Figure E7.6.1 at the region on top of the wire with particle of 3.3 μm radius, showing the magnetic force density in the downward direction displayed in contours of N/m^3 using the scale shown. For color display see website http://ieeexplore.ieee.org/ for [21].

TABLE E7.6.1 Magnetic Forces Computed by Force Density Integration on Particles Centered at Radius 3.3 μm From Wire of Radius 10 μm, Both With Relative Permeability 1000 in 1 T Field

Particle Radius (μm)	Cylindrical Particle (N/m)	Spherical Particle (N)
0.1	3.072E–3	401.9E–12
1.0	0.3128	427.0E–9
2.0	1.2314	3.503E–6
3.3	3.591	14.57E–6

here carried out on the magnetic force density displayed in Figure E7.6.2 for various particles of radius in the micrometer and nanometer range. The resulting forces are listed in Table E7.6.1. Because of known accuracy problems with Maxwell stress computations [22], only the 0.1 μm radius cylindrical case was checked by Maxwell stress, which obtained force in the range of 10E–3 N/m to 3.6E–3 N/m depending on the finite-element mesh used.

Dividing the forces of Table E7.6.1 by the volumes of the cylindrical and spherical particles, the computed average force densities are obtained and plotted versus particle radius in Figure E7.6.3. Note that they are all slightly smaller than the theoretical density obtained by the approximate Oberteuffer formula. Note, however, that in all cases the finite-element computations agree reasonably well with Oberteuffer, within −8.46 to −0.12%.

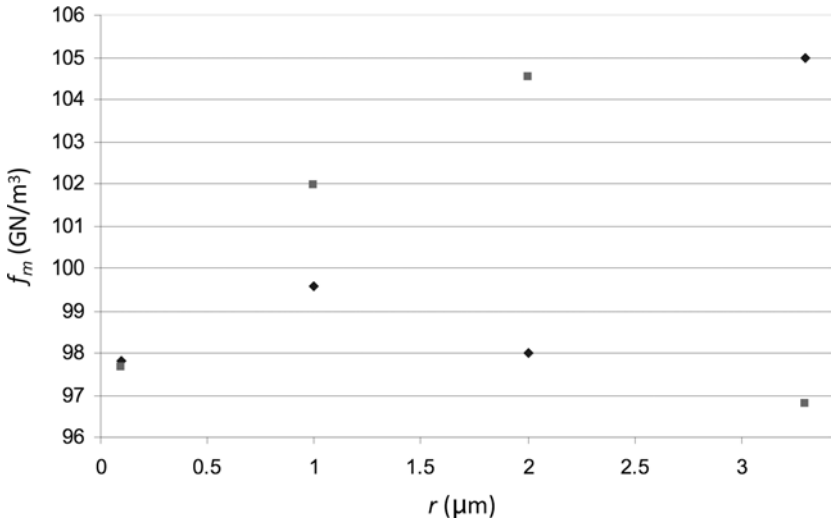

FIGURE E7.6.3 Plot of volume-average magnetic force densities computed in Table E7.6.1 versus radius for cylinders (diamonds) and spheres (squares) as data points compared to approximate Oberteuffer density constant value of 105.75E9 N/m^3. Note that the vertical scale is zoomed; the difference between computed data points and Oberteuffer varies from −8.46% to −0.1%.

Besides mineral separation using magnetic field gradients [23–25], a rapidly growing area of magnetic separation is for medical devices and biomolecular screening including DNA testing. High field gradient magnetic separation is used to separate red blood cells from blood and cancer cells from bone marrow. Other biomedical magnetic actuators are being investigated to target drug delivery and to remove toxins [26]. As mentioned previously, permanent magnets are often used as a field source for magnetic separators. They are being investigated for biomolecular screening using standard biomolecular testing apparatus.

Example 7.7 Force Density of a Permanent Magnet Separator on a Biomolecular Microplate For drug discovery, DNA/RNA testing, detection of proteins/antigens/genes, and other types of biomolecular screening, a standard tool is the microplate [27], which typically contains 96 wells as shown in Figure E7.7.1. One

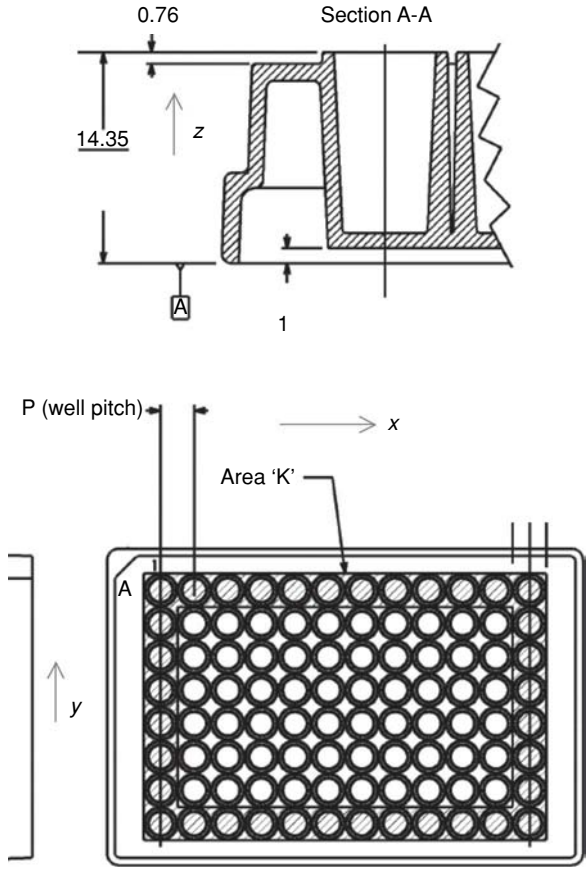

FIGURE E7.7.1 View of 96-well microplate for biomolecular screening [27]. The lower view shows the entire microplate in the horizontal *xy* plane. The upper view is a detailed section showing one well in the *xz* plane. Dimensions are in mm, and standard well pitch is 9 mm. Microplate materials have the magnetic permeability of air.

screening method is to place in each well, a solution with suspended permeable microparticles, often spherical beads. By coating the permeable microparticles with different proteins or other biological molecules [26, 28] in each well, magnetic separation enables biomolecular screening. Thus such microparticles can serve as magnetic sensors [29, 30]. Spherical microparticle diameters are often in the range of 1–4 μm, but may be reduced to nanometers. Here the magnetic force density acting on such particles is to be computed with finite-element software in one of the wells of Figure E7.7.1 with a permanent magnet separator immediately above it. The permanent magnet is first made of ferrite and next made of neodymium iron boron.

Solution The top region of one well of Figure E7.7.1 is shown in Figure E7.7.2 along with an adjacent well. Also shown is the magnetic flux plot computed using Maxwell for a cylindrical permanent magnet placed just above the well of primary interest. The flux lines are computed using axisymmetric finite-element analysis because the permanent magnet and the well below it all have axisymmetric geometry. The axisymmetric plane has the z axis vertical (in the same direction as z axis of Figure E7.7.1) and the radial r axis (which can be aligned with the x axis of Figure E7.7.1) horizontal.

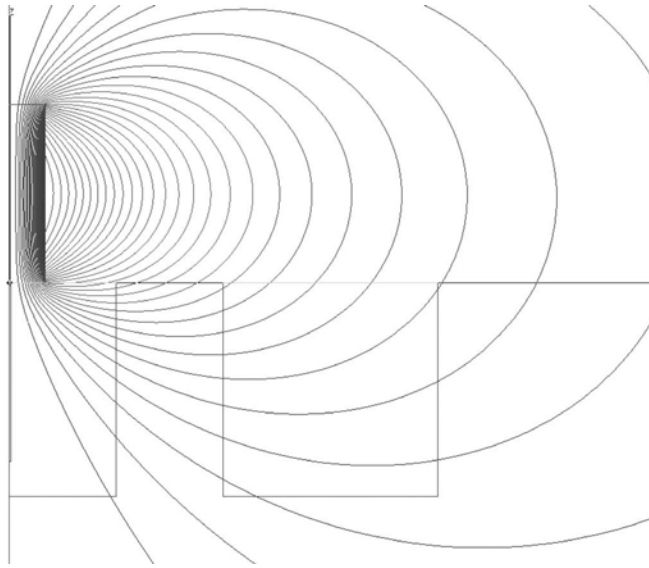

FIGURE E7.7.2 Two wells of Figure E7.7.1 modeled in the axisymmetric rz plane with a cylindrical permanent magnet above them. The left rectangle outlines the top of the well of primary interest, with a height 6 mm and radius 3 mm. The right rectangle models an adjacent well top of the same size (height 6 mm and diameter 6 mm). The centerlines of both wells are separated by 9 mm, agreeing with the standard microplate of Figure E7.7.1. Also shown are the flux lines computed by Maxwell axisymmetric finite-element analysis.

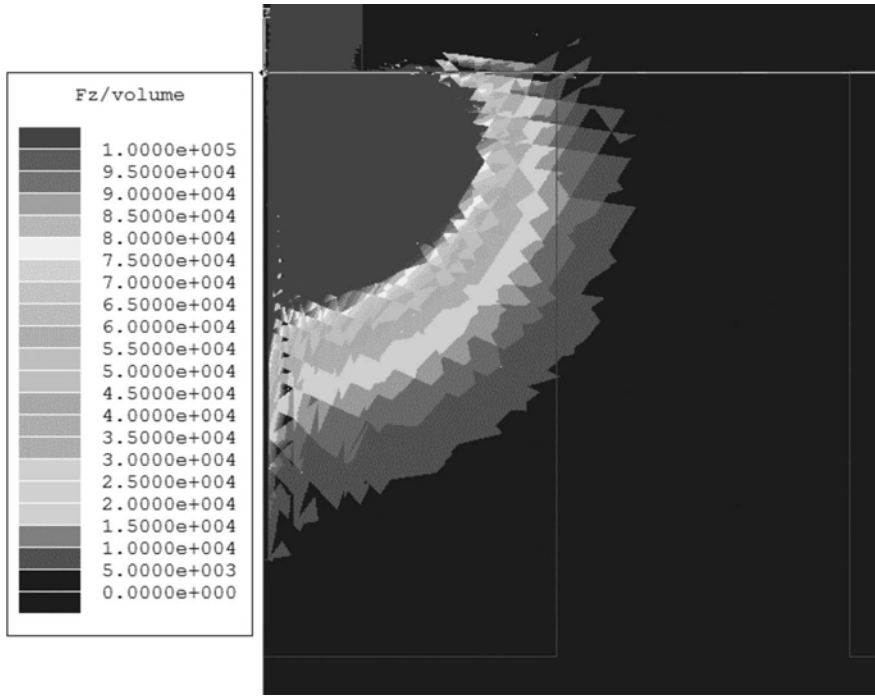

FIGURE E7.7.3 The vertical magnetic force density in N/m^3 computed for Figure E7.7.2 below the magnet made of ferrite. This zoomed plot shows the entire primary well top along with the left edge of the adjacent well top.

The computed vertical z-directed magnetic force density distribution is displayed in Figures E7.7.3 and E7.7.4 for two different permanent magnet separators. The vertical magnetic force density is upward against gravity, and thus must exceed gravitational and buoyancy forces for successful separation. The gravitational force density is:

$$f_{gz} = -\rho g \tag{E7.7.1}$$

which is in the $-z$ direction, where ρ is the mass density and g is the acceleration of gravity. Since in SI units $g = 9.8$ kg m/s^2 and $\rho = 1000\rho_s$ kg/m^3, where ρ_s is specific gravity, the gravitational force density is:

$$f_{gz} = -9.8E3\rho_s \tag{E7.7.2}$$

For iron, specific gravity $\rho_s = 7.8$, giving $f_{gz} = -7.644$E4 N/m^3. For microparticles placed in solution in the microplate wells of Figures E7.7.1 and E7.7.2, ρ_s is less than that of iron because such particles are made of iron oxide mixed with polymers. Because of this mixture, the permeability of the microparticles is also reduced from that of iron.

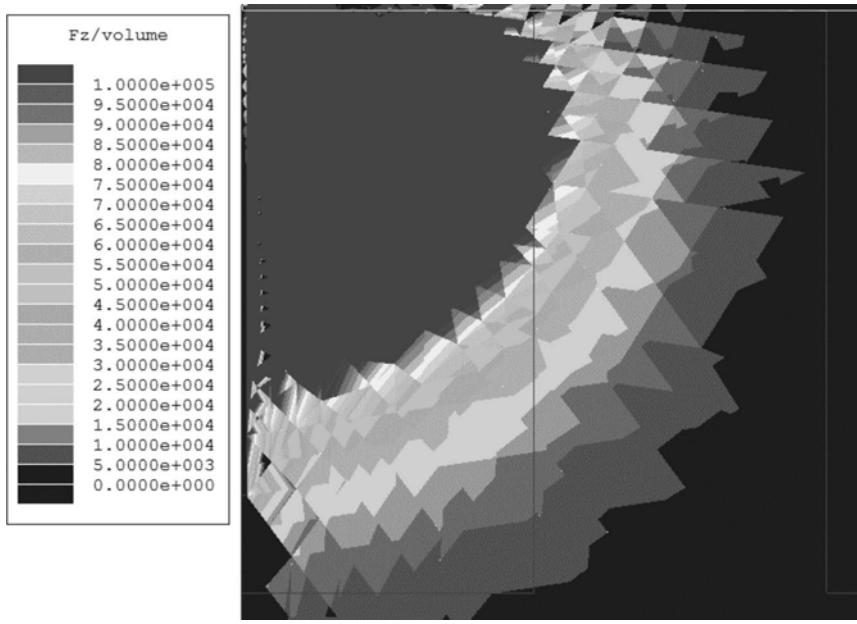

FIGURE E7.7.4 The vertical magnetic force density in N/m^3 computed for Figure E7.7.2 below the magnet made of NdFeB. This zoomed plot shows the entire primary well top along with the left edge of the adjacent well top. Note that the stronger magnet produces a higher force density.

Microparticle specific gravity and permeability are either unknown or proprietary and thus cannot be reported here. However, since both are substantially lower than that of iron, both the gravitational force density of (E7.7.2) and the magnetic force density of (5.32) are reduced from those of iron. Thus for comparison both forces are computed here using the properties of iron. The relative permeability of the iron is assumed to be 1000 or higher, since such high μ_{rp} is shown by (5.32) to produce force variations of 0.1% or less.

For the permanent magnet separator of Figure E7.7.2 to function properly, the magnetic force density in the primary well must exceed downward force density. The downward force density is the vector sum of gravitational, buoyancy, viscous, and surface tension force densities. Here the gravitational force is assumed to dominate. Since the gravitational force density is of magnitude 7.644E4 N/m^3, the magnetic force density will be displayed in the range from 0 to 1.E5 N/m^3.

Figures E7.7.3 and E7.7.4 display the vertical magnetic force densities computed using (5.32) for two different permanent magnet separators in Figure E7.7.2. In both cases the permanent magnet is assumed to have radius 1 mm and length 5 mm, as shown in Figure E7.7.2.

In Figure E7.7.3 the permanent magnet is assumed to be made of ceramic 5 ferrite with coercive field intensity H_c = 1.91E5 A/m and relative permeability = 1.08.

The vertical magnetic force density display shows that the 1.E5 N/m^3 zone is much smaller than the primary well. Thus over most of the well the magnetic force density is insufficient to overcome the gravitational force density.

In Figure E7.7.4 the permanent magnet is instead assumed made of neodymium iron boron (NdFeB) with $H_c = 8.9E5$ A/m and relative permeability = 1.1. The vertical magnetic force density now has a 1.E5 N/m^3 zone that is large enough to encompass most of the primary well top, without intruding into the adjacent well. Thus the magnetic force density overcomes the gravitational force density in most of the primary well while not interfering with the adjacent well, resulting in proper magnetic separation in the microplate.

In actual microplate magnetic separation, it is known that NdFeB permanent magnets with $H_c \sim 8.9E5$ A/m are required. Thus the computed results of Figures E7.7.3 and E7.7.4 agree qualitatively with observed behavior. The finite-element method computations can readily analyze many other designs of magnetic separators made of permanent magnets, steel, and other materials.

PROBLEMS

7.1 Assume the planar solenoid with a clapper armature shown in Figure E7.1.1 has the following dimensions: $w = 12$ mm, $Al_1 = 6$ mm, $Al_2 = 40$ mm, $Al_3 = 6$ mm, $Sl_1 = 20$ mm, $Sl_2 = 40$ mm, $Sl_3 = 20$ mm, $g = 1$ mm. It also has $N = 300$ and $I = 2$ A.

Use the reluctance method, assuming no leakage or fringing fluxes, to find the approximate values of the following.

(a) Vector **B** and **F** on left side of clapper.

(b) Vector **B** and **F** on right side of clapper.

(c) Obtain the above answers with Maxwell finite-element software by using high permeability material (relative permeability = 2000) in the steel.

(d) Obtain the answers for the above with finite-element software with steel relative permeability = 10,000, and comment on why the results differ.

(e) Repeat (c) for $I = 2$, 3, and 4 and the airgap $g = 0.5$ mm, 1 mm, 1.5 mm, 2 mm, 2.5 mm, 3 mm, 3.5 mm, and 4 mm and plot the resulting pull curves.

7.2 The axisymmetric solenoid with a clapper armature shown in Figure E7.2.1 has the following dimensions: $g = 1$ mm, $w_a = 7$ mm, $R_1 = 15$ mm, $R_2 = 25$ mm, $R_3 = 30$ mm, $Z_1 = 7$ mm, and $Z_2 = 23$ mm. It also has $N = 1500$ and $I = 1$ A.

Use the reluctance method, assuming no leakage or fringing fluxes, to find the approximate values of the following.

(a) **B** and **F** on inside of clapper.

(b) **B** and **F** on outside of clapper.

(c) Obtain the above answers with finite-element software by using high permeability material (relative permeability = 2000) in the steel.

(d) Obtain the answers for the above with finite-element software with steel relative permeability = 10,000, and comment on why the results differ.

7.3 The planar solenoid with a plunger armature shown in Figure E7.3.1 has the following dimensions: $w = 8$ mm, $g = 3$ mm, $g_s = 1.5$ mm, $Al_1 = 4$ mm, $Al_2 = 22$ mm, $Sl_1 = 8$ mm, $Sl_2 = 20$ mm, $Sl_3 = 34$ mm, and $Sl_4 = 15$ mm. It also has $N = 800$ and $I = 2$ A.

(a) Use the reluctance method, assuming no leakage flux, to find the approximate values of **B** and **F** on the end of the plunger.

(b) Compute the above **B** and **F** using finite-element software with the relative permeability = 2000 in the steel.

(c) Obtain the answers for the above with finite-element software with steel relative permeability = 10,000, and comment on why the results differ.

7.4 The axisymmetric solenoid with a plunger armature shown in Figure E7.4.1 has the following dimensions: plunger and pole outer radius $R_P = 18$ mm, side airgap outer radius $R_{PG} = 20$ mm, stator yoke outer radius $R_{YO} = 70$ mm, stator yoke inner radius $R_{YI} = 66$ mm, working airgap $g = 8$ mm, plunger length $L_P = 42$ mm, stator stopper length $L_S = 16$ mm, coil axial length $L_C = 46$ mm, and stator yoke axial thickness $t = 12$ mm (on top, same on bottom). It also has $N = 400$ and $I = 3$ A.

(a) Use the reluctance method, assuming no leakage flux, to find the approximate values of **B** and **F** on the end of the plunger.

(b) Compute the above **B** and **F** using finite-element software, with the relative permeability = 2000 in the steel.

(c) Obtain the answers for the above with finite-element software with steel relative permeability = 10,000, and comment on why the results differ.

7.5 A voice coil has a resistance of 15 Ω and 300 turns. A permanent magnet provides a DC magnetic flux density of 0.6 T in the radial r direction. The average radius r of the voice coil is 20 mm. If 10 volts DC is applied to the voice coil, find the steady-state vector force produced.

7.6 A voice coil lies from radius 10 mm to 14 mm. It has 200 turns and a resistance of 20 Ω. It is subjected to a DC magnetic flux density of 0.5 T in the radial r direction. If 6 volts DC is applied to the coil, find its steady-state vector force.

7.7 A proportional actuator is made of a voice coil actuator with $F = 100I$ and a spring with $F_s = 1.E5x$ in opposition. On a graph of total force versus x, for $x = 0$–0.010 m, draw the force lines for I varying from –1 A to +10 A in 1 A increments.

7.8 A step motor has 10 stator teeth and 8 rotor teeth. Find its incremental (step) angle of motion.

REFERENCES

1. Jay F (ed.). *IEEE Standard Dictionary of Electrical and Electronics Terms*, 2nd ed. New York, NY: Wiley-Interscience; 1977.
2. Juds MA, Brauer JR. AC contactor motion computed with coupled electromagnetic and structural finite elements. *IEEE Trans Magn* 1995;31:3575–3577.
3. Bessho K, Yamada S, Kanamura Y. Analysis of transient characteristics of plunger type electromagnets. *Electr Eng Jpn* 1978;98:56–62.
4. Yoon SB, Hur J, Chun YD, Hyun DS. Shape optimization of solenoid actuator using the finite element method and numerical optimization technique. *IEEE Trans Magn* 1997;33:4140–4142.
5. Brauer JR (ed.). *What Every Engineer Should Know About Finite Element Analysis*, 2nd ed. New York: Marcel Dekker, Inc.; 1993. Chapter 7, Design Optimization, by R. S. Lahey.
6. Ratliffe RT, Pagilla PR. Design, modeling, and seek control of a voice-coil motor actuator with nonlinear magnetic bias. *IEEE Trans Magn* 2005;41:2180–2188.
7. Lequesne B. Fast acting, long-stroke solenoids with two springs. *IEEE Trans Industry Appl* 1990;26:845–856.
8. Lequesne B. Permanent magnet linear motors for short strokes. *IEEE Trans Industry Appl* 1996;32:161–168.
9. Lequesne B. Fast acting, long-stroke bistable solenoids with moving permanent magnets. *IEEE Trans Industry Appl* 1990;26:401–407.
10. Lequesne B. Finite element analysis of a constant force solenoid for fluid flow control. *IEEE Trans Ind Appl* 1988;24:574–581.
11. Brauer JR, Aronson EA, McCaughey KG, Sullivan WN. Three dimensional finite element calculation of saturable magnetic fluxes and torques of an actuator. *IEEE Trans Magn* 1988;24:455–458.
12. Iannello V. *Advances in Magnetic Bearings*, Brochure from Synchrony Division of Dresser-Rand, Salem, VA, 2009 (excerpted by permission).
13. Chen SL, Chen SH, Yan ST. Experimental validation of a current-controlled three-pole magnetic rotor-bearing system. *IEEE Trans Magn* 2005;41:99–112.
14. Tian L-L, Ai X-P, Tian Y-Q. Analytical model of magnetic force for axial stack of permanent magnet bearings. *IEEE Trans Magn* 2012;48:2592–2599.
15. Bachovchin KD, Hoburg JF, Post RF. Stable levitation of a passive magnetic bearing. *IEEE Trans Magn* 2013;49:609–617.
16. Wu W, Lovatt HC, Dunlop JB. Analysis and design optimization of magnetic couplings using 3D finite element modeling. *IEEE Trans Magn* 1997;33:4083–4085.
17. Kamm LJ. *Understanding Electro-Mechanical Engineering*. New York: IEEE Press; 1996.
18. Kallenbach E, Eick R, Quendt P, Ströhla T, Feindt K, Kallenbach M. In: Teubner BG (ed.), *Elektromagnete*, 2nd ed. Wiesbaden, Germany: Verlag/Springer; 2003 (in German).
19. Rosensweig RE. *Ferrohydrodynamics*. Mineola, NY: Dover Publications; 1985.
20. Oberteuffer JA. Magnetic separation: a review of principles, devices, and applications. *IEEE Trans Magn* 1974;10:223–238.
21. Brauer JR, Cook DL, Bray TE. Finite element computation of magnetic force densities on permeable particles in magnetic separators. *IEEE Trans Magn* 2007;43:3483–3487.

22. Burow DW, Salon SJ. Dependence of torque calculation on mesh in induction machines. *IEEE Trans Magn* 1995;31:3593–3595.
23. Gerber R, Birss R. *High Gradient Magnetic Separators*. New York: John Wiley & Sons; 1984.
24. Smolkin MR, Smolkin RD. Calculation and analysis of the magnetic force acting on a particle in the magnetic field of a separator. Analysis of the equations used in the magnetic methods of separation. *IEEE Trans Magn* 2006;42:3682–3693.
25. Hoffmann C, Franzreb M. A novel repulsive-mode high gradient magnetic separator—I. Design and experimental results. *IEEE Trans Magn* 2004;40:456–461.
26. Hoffman A. Magnetic viruses for biological and medical applications. *Magn Bus & Technol* 2005;24 ff.
27. Standard 2-2004 for Microplates, American National Standards Institute/Society for Biomolecular Sciences (March 28, 2005).
28. Brauer JR. Modeling force density distributions on biomolecular nanoparticles undergoing magnetic separation. *Magnetics Bus & Technol* 2008;26–27.
29. Fodil K, Denoual M, Dolabdjian C, Harnois M, Senez V. Dynamic sensing of magnetic nanoparticles in microchannel using GMI technology. *IEEE Trans Magn* 2013;49:93–96.
30. Eberbeck D, Dennis CL, Huls NF, Krycka KL, Gruttner C, Westphal F. Multicore magnetic nanoparticles for magnetic particle imaging. *IEEE Trans Magn* 2013;49:269–274.